Cluster dynamics studied with the phase-space minimum spanning tree approach

Viktar Kireyeu
Joint Institute for Nuclear Research, Joliot-Curie 6, 141980 Dubna, Moscow region, Russia
and Helmholtz Forschungsakademie Hessen für FAIR (HFHF), GSI Helmholtzzentrum für Schwerionenforschung, Campus Frankfurt, Max-von-Laue-Str. 12, 60438 Frankfurt am Main, Germany

(Received 18 March 2021; accepted 3 May 2021; published 17 May 2021)

The origin of weakly bound objects like clusters and hypernuclei, observed in heavy-ion collisions, is of theoretical and experimental interest. It is in the focus of the experiments at the BNL Relativistic Heavy Ion Collider (RHIC) and the Large Hadron Collider (LHC) since it is not evident how such weakly bound objects can survive in an environment whose hadronic decay products point to a temperature of the order of 150 MeV. It is also one of the key research topics in the future facilities of FAIR and NICA, which are under construction in Darmstadt (Germany) and Dubna (Russia), respectively. The first results on the cluster dynamics within the model-independent cluster recognition library "phase-space minimum spanning tree" (psMST) applied to different transport approaches: PHQMD, PHSD, SMASH, and UrQMD are presented here. The psMST is based on the "minimum spanning tree" (MST) algorithm for the cluster recognition which exploits correlations in coordinate space, and it is extended to correlations of baryons in the clusters in momentum space. The sensitivity of the cluster formation on the microscopic realization of the n-body dynamics and on the potential interactions in heavy-ion collisions is shown.

DOI: 10.1103/PhysRevC.103.054905

I. INTRODUCTION

Novel accelerator complexes provide us with the interesting possibility to produce and to study a new type of matter which cannot exist under the "normal" conditions—the quark-gluon plasma (QGP). A "soup" of quarks and gluons, which existed at the first microseconds after the Big Bang, can be created at facilities like the BNL Relativistic Heavy Ion Collider (RHIC) and the Large Hadron Collider (LHC). In future experiments at lower energy, at the Nuclotron based Ion Collider Facility (NICA) in Dubna and at the Facility for Antiproton and Ion Research (FAIR) in Darmstadt, extend these experiments toward strongly interacting matter of high net baryon density [1].

Cluster and hypernuclei production, experimentally observed in a wide energy range [2–12], is interesting for several reasons: first of all, the mechanism of cluster formation in nucleus-nucleus collisions is not well understood and requires further investigations. For deuterons and tritons having a small binding energy (of several MeV) compared with freeze-out temperature (around 100–150 MeV), it is very unlikely that they will survive a collisions with another hadron. Consequently, it is most probable that the observed deuterons and tritons, as well as the significant fraction of few-nucleon bound states registered near midrapidity, are produced in the late stage of the reaction close to the freeze-out point. Thus, the light nuclei, observed in the experiment and formed near the freeze-out, may provide information on the space-time structure of this late stage of the collision. The capture of the produced hyperons by clusters of nucleons leads to hypernucleus formation, which is a very rare process at strangeness threshold energies. Hypernuclei are a unique probe for improving our knowledge on the strange particle-nucleon interaction in a many-body environment and under the controlled conditions. The theoretical description of the cluster and hypernuclei formation is quite sensitive to the strange baryon-nucleon interaction, which can therefore be tested in such heavy-ion collisions.

Most of the transport approaches, developed for the dynamical description of heavy-ion collisions, use statistical [13,14] or coalescence models [15–18] to describe the cluster formation, or omit it. Recently these approaches were applied to the ultrarelativistic quantum molecular dynamics approach [19,20]. Another possibility is to use the "Minimum Spanning Tree" (MST) [21] procedure. While the coalescence model requires a multitude of parameters for each isotope, the MST uses only the coordinate space information of the baryons to identify clusters at the end of the reaction when free and bound nucleons are well separated in space.

To overcome the MST limitation that clusters can be formed only at the end of reaction, the simulated annealing clusterization algorithm (SACA) [22,23] was developed based on the idea of Dorso and Randrup [24] that the most-bound configurations of clusters and free nucleons identified during the collision evolution have a large overlap with the final distribution of clusters and free nucleons. Thus, SACA can be applied to identify clusters at earlier times, shortly after the passing time, when interactions between nucleons are still ongoing and the nuclear density is high. For each possible configuration of clusters and unbound nucleons, SACA

calculates the total binding energy (neglecting interactions among clusters). The most-bound configuration is found by the simulated annealing technique using a "metropolis" algorithm. An extended version of SACA, the "fragment recognition in general application" (FRIGA) [25] is under development now. The FRIGA includes the symmetry and the pairing energy as well as hyperon-nucleon interactions.

The extended study of cluster formation mechanisms within the MST and SACA procedures have been performed recently by employing the parton-hadron-quantum-molecular dynamics approach [26]. In this study, the importance of the dynamical n-body description of the nucleon-nucleon interactions has been demonstrated. It allows us to conserve spatial and momentum correlations of nucleons and hyperons, which yields to the dynamical formation of (hyper)nuclei, which later on can be recognized by MST and SACA.

The application of the MST ideas to other transport models would extend our understanding on the cluster formation and on the consequences of different realizations of nucleon-nucleon interactions. In particular, it allows us to study whether the n-body quantum-molecular dynamics (QMD) approach provides for clusters at midrapidity different results than approaches in which the one-body phase-space density is propagated or which do not at all include potential interactions. Furthermore, this also allows us to study the impact of different matter equations of state (EoS) on the cluster-formation process.

Therefore the use of the "phase-space minimum spanning tree" (psMST) approach is advanced for the simulation of the cluster production, which can be applied to any transport model and allow addressing multiple physics phenomena in the (hyper)nuclei formation process. In addition, it can be also used for numerous feasibility study tasks for future experimental setups at NICA and FAIR.

This paper is organized as follows: in Sec. II a description of the psMST library is provided. A brief description of transport approaches to which psMST is applied is presented in Sec. III. First results for the cluster formation using psMST for four transport approaches are shown in Sec. IV. Finally, the conclusions are presented in Sec. V.

II. PHASE-SPACE MINIMUM SPANNING TREE

The phase-space minimum spanning tree (psMST) is based on the idea of the MST algorithm for searching bound nucleon systems in dense hadronic matter [21,26]. Since it is an independent library, it can be applied to all transport models which propagate hadrons. This includes models based on n-body dynamics like the different flavors of the quantum-molecular dynamics (QMD) approach as well as models based on mean-field (MF) dynamics or cascade approaches in which no potential interactions between nucleons takes place. Thus, a model + psMST combination allows us to study the impact of particular realization of nuclear dynamics on the clusters formation process. Moreover, in addition to the spatial correlations used in the default MST version for cluster recognition, psMST can be used to study the influence of the momentum correlations of nucleons and hyperons for the formation of (hyper)nuclei. The psMST library is open-source code [27], which can be used either in stand-alone mode or can be integrated in any software framework for detector simulation and analysis.

In this work three different scenarios of using the psMST library are studied:

(1) Scenario 1. Similar to the MST procedure, the psMST algorithm is only dealing with the coordinate information to find clusters: a pair of particles (i, j) forms a cluster if the distance between candidates is less than the "clusterization" radius which is chosen to be $r_{\rm clust} = 4$ fm, i.e., $\Delta r \leqslant r_{\rm clust}$. The distance Δr is calculated in the pair center of mass frame. Moreover, a particle is assigned to the existing cluster if it meets the same condition as above with at least one particle of the cluster. In this mode, psMST results are identical to the original MST procedure.

(2) Scenario 2. The first step is identical to scenario 1, but then, once all possible combinations for clusters are found, an additional momentum cut is applied for candidates. First, the cluster velocity is calculated as

$$\mathbf{V} = \frac{\sum_{i=1}^{n} \mathbf{p_i}}{\sum_{i=1}^{n} E_i}, \tag{1}$$

where $\mathbf{p_i}$, E_i are the ith particle momentum and energy in the calculational frame of heavy-ion collisions (which is often taken as the $N + N$ center-of-mass frame), and n is the number of particles assigned to the cluster. Then the momentum of each particle assigned to the cluster is boosted to the cluster center-of-mass frame by the corresponding Lorentz transformation with the velocity $\mathbf{V}$:

$$\mathbf{p}' = L(\mathbf{V})\mathbf{p}. \tag{2}$$

In this scenario the momentum cut is applied for all found clusters in order to investigate the deviation of their momentum distribution from the Fermi momentum distribution expected for stable clusters. A cluster is excluded from the analysis if at least one its particle has a momentum $\mathbf{p}' > 300$ MeV in the cluster rest system.

(3) Scenario 3. In this scenario the clusterization criterion of the spatial MST (scenario 1) is extended by a cut in momentum space depending on the relative momentum of cluster particles:
   (a) As in scenario 1, the algorithm is looking first for the coordinate-space information. Particles are selected as cluster candidates if the distance between two particles (i, j) (or with at least one particle of the cluster in case of an already existing cluster) $\Delta r \leqslant r_{\rm clust}$. The distance Δr is calculated in the particles pair center-of-mass frame $(i + j)$.
   (b) Then an additional momentum cut is applied to each particle: a particle can be added to the cluster only if each particle of this cluster has a relative momentum $\mathbf{p}' < 300$ MeV in the cluster center-of-mass frame. This procedure is repeated after a new particle is assigned to the cluster after the proximity Δr check.

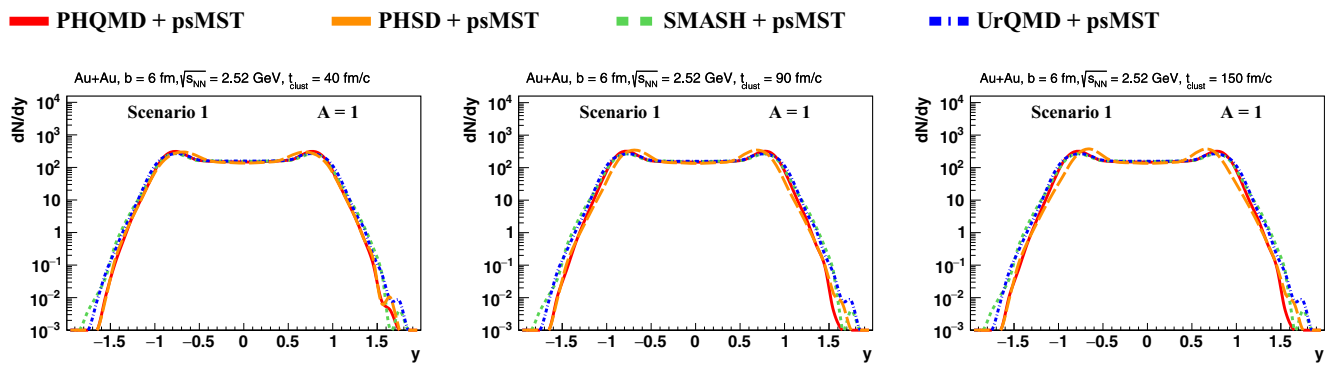

FIG. 1. The rapidity distributions of unbound baryons (p, n, Λ, and Σ^0) in semiperipheral ($b = 6$ fm) Au + Au collisions at $\sqrt{s} = 2.52$ GeV. The y distributions at (left panel) 40 fm/c, at (central panel) 90 fm/c, at (right panel) 150 fm/c. The red solid lines show the PHQMD results, the orange long dashed lines indicate the PHSD results, the green dashed lines correspond to the SMASH results, and the blue dot-dashed lines correspond to the UrQMD results.

Contrary to scenario 2, the momentum cut is applied during the clusterization procedure. This leads to a different cluster distribution since the particles rejected from one cluster by the momentum cut can become a member of another cluster.

III. APPLICATION OF THE PHASE-SPACE MINIMUM SPANNING TREE TO TRANSPORT MODELS

To study the similarity and possible differences of the cluster formation within different transport models (based on mean-field, cascade, or QMD dynamics) the psMST algorithm was applied to four transport approaches: PHSD-4.0, PHQMD-2.0, SMASH-2.0 and UrQMD-3.4 at two energies $\sqrt{s_{NN}} = 2.52$ GeV and $\sqrt{s_{NN}} = 8.8$ GeV. The basic ideas of these approaches are briefly mentioned here.

The parton-hadron-string dynamics (PHSD) [28,29] is a microscopic off-shell transport approach that describes the evolution of a relativistic heavy-ion collision from the initial hard scatterings and string formation through the dynamical deconfinement phase transition to the quark-gluon plasma as well as hadronization and the subsequent interactions in the hadronic phase. It is based on the solution of Kadanoff–Baym equations in a first-order gradient expansion employing "resummed" propagators from the dynamical quasiparticle model (DQPM) [30,31] for the partonic phase. At lower energies it reduces to a hadronic transport model. PHSD incorporates a density-dependent Skyrme potential at low (SIS) energies and the covariant momentum dependent potential at high energies.

The parton-hadron-quantum-molecular dynamics (PHQMD) [26] is an n-body dynamical transport approach which is designed to provide a microscopic dynamical description for the formation of light and heavy clusters and hypernuclei as well as for hadrons in relativistic heavy-ion collisions. The propagation of baryons is based on the n-body QMD dynamics while the description of mesons and of the QGP dynamics as well as the collision integral was taken from the PHSD model. The PHQMD includes mutual two-body density-dependent Skyrme-type potentials for the interaction among baryons. The attractive interaction binds clusters with a binding energy of about 8 MeV/N.

The simulating many accelerated strongly interacting hadrons (SMASH) [32,33] model is a hadronic transport approach which provides a dynamical description of heavy-ion reactions in the low and intermediate beam-energy range. The relativistic Boltzmann equation with hadronic degrees of freedom is solved including an (optional) density-dependent Skyrme-type mean-field potential. In this study the SMASH model is used in its default version without potential.

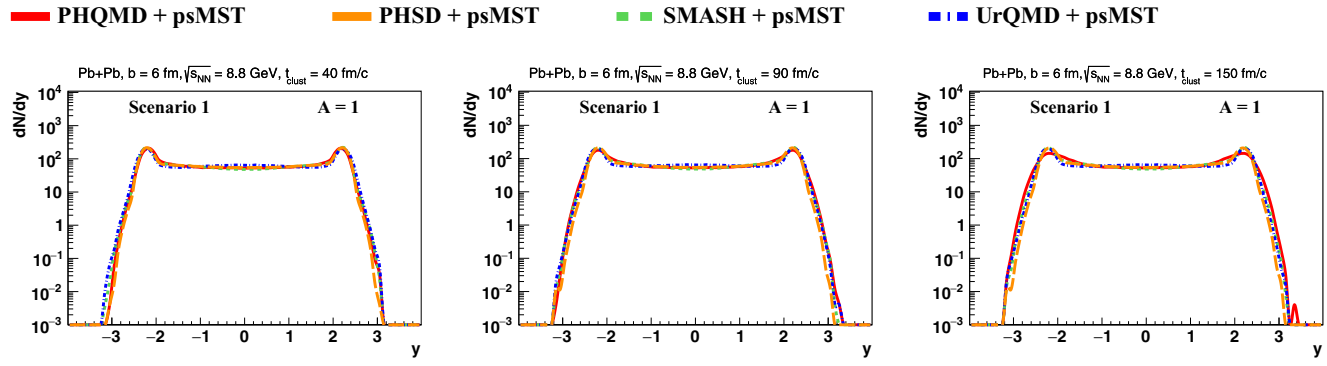

FIG. 2. The rapidity distributions of single baryons (p, n, Λ, and Σ^0) in semiperipheral ($b = 6$ fm) Pb + Pb collisions at $\sqrt{s} = 8.8$ GeV. The y distributions at (left panel) 40 fm/c, at (central panel) 90 fm/c, at (right panel) 150 fm/c. The color coding is the same as in Fig. 1.

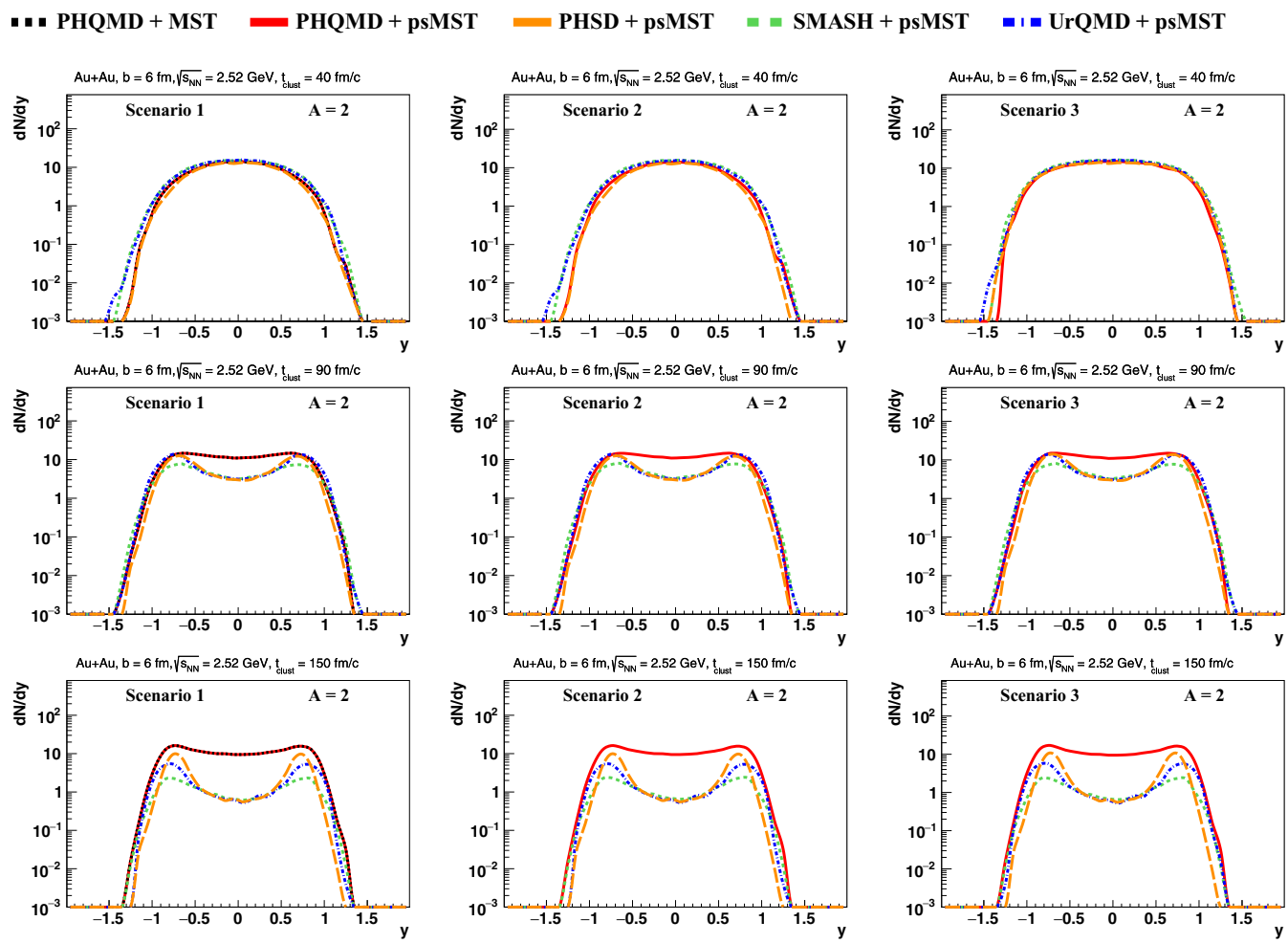

FIG. 3. The rapidity distributions of the clusters with the mass number $A = 2$ in semiperipheral ($b = 6$ fm) Au + Au collisions at $\sqrt{s} = 2.52$ GeV. The left column shows scenario 1, the central column shows scenario 2, the right column shows scenario 3 (see text). The black short dashed lines (PHQMD + MST) show the PHQMD results at time $t_{\rm clust}$ within the MST cluster recognition model, the red solid lines show the PHQMD results within psMST, the orange long dashed lines indicate the PHSD results within psMST, the green dashed lines correspond to the SMASH results within psMST, the blue dot-dashed lines show the UrQMD results within psMST. The upper row corresponds to the model calculations at $t_{\rm clust} = 40$ fm/c, the middle row at $t_{\rm clust} = 90$ fm/c, and the lower row at $t_{\rm clust} = 150$ fm/c.

The ultrarelativistic quantum molecular dynamics (UrQMD) [34,35] model is a microscopic transport approach which describes hadronic reactions at low and intermediate energies in terms of collisions among hadrons and their resonances. At higher energies the multiparticle production within UrQMD model is dominated by the excitation of color strings and their subsequent fragmentation into hadrons. The default version of UrQMD without potentials was used here.

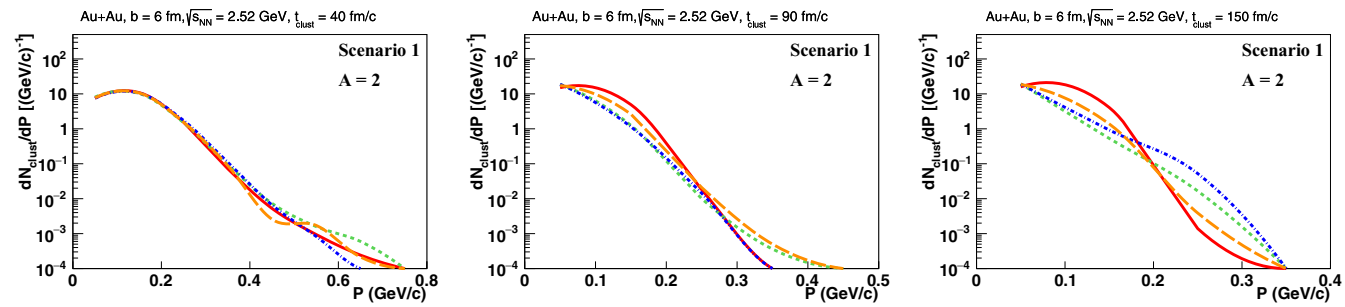

FIG. 4. The momentum spectra of baryons (p, n, Λ, and Σ^0) from $A = 2$ clusters in semiperipheral ($b = 6$ fm) Au + Au collisions at $\sqrt{s} = 2.52$ GeV (integrated over all rapidity range). The momentum is calculated in the cluster center of mass frame. The left column shows $t_{\rm clust} = 40$ fm/c, the central column shows $t_{\rm clust} = 90$ fm/c, the right column shows $t_{\rm clust} = 150$ fm/c. The color coding is the same as in Fig. 3.

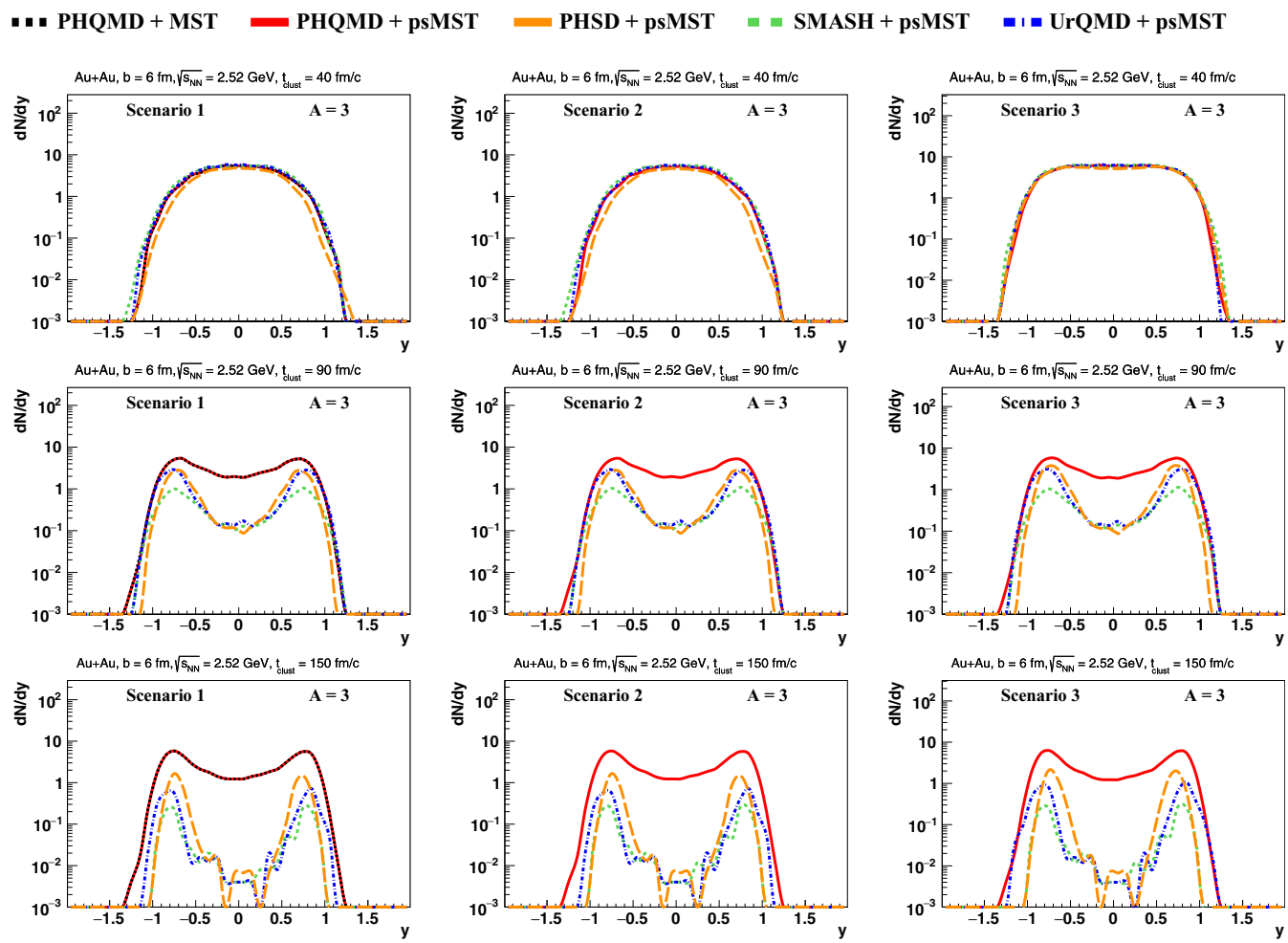

FIG. 5. The rapidity distributions of clusters with the mass number $A = 3$ at $t_{\rm clust} = 40, 90, 150$ fm/c in semiperipheral ($b = 6$ fm) Au + Au collisions at $\sqrt{s} = 2.52$ GeV. The left column shows scenario 1, the center column shows scenario 2, the right column shows scenario 3. The color coding is the same as in Fig. 3.

Thus, in this study several different models are used: one model based on quantum-molecular dynamics (PHQMD with a Skyrme potential for baryons), one mean-field model (PHSD, based on the Kadanoff–Baym equation including potentials for baryons), and two cascade approaches (UrQMD and SMASH). The psMST algorithm is applied to "snapshots" from these models at different times and compare the results for the yields of clusters. A snapshot means that, at a given time, all coordinates and momenta of all baryons are stored for a further psMST analysis. It should be pointed out that all resonance states are excluded from the cluster recognition process. However, the standard output from SMASH and

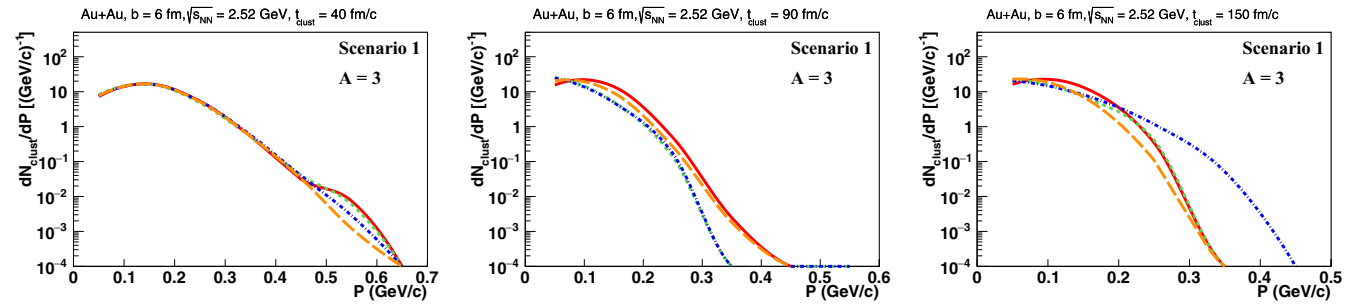

FIG. 6. The momentum spectra of baryons (p, n, Λ, and Σ^0) from $A = 3$ clusters in semiperipheral ($b = 6$ fm) Au + Au collisions at $\sqrt{s} = 2.52$ GeV (integrated over all rapidity range). The momentum is calculated in the cluster center-of-mass frame. The left column shows $t_{\rm clust} = 40$ fm/c, the center column shows $t_{\rm clust} = 90$ fm/c, and the right column shows $t_{\rm clust} = 150$ fm/c. The color coding is the same as in Fig. 3.

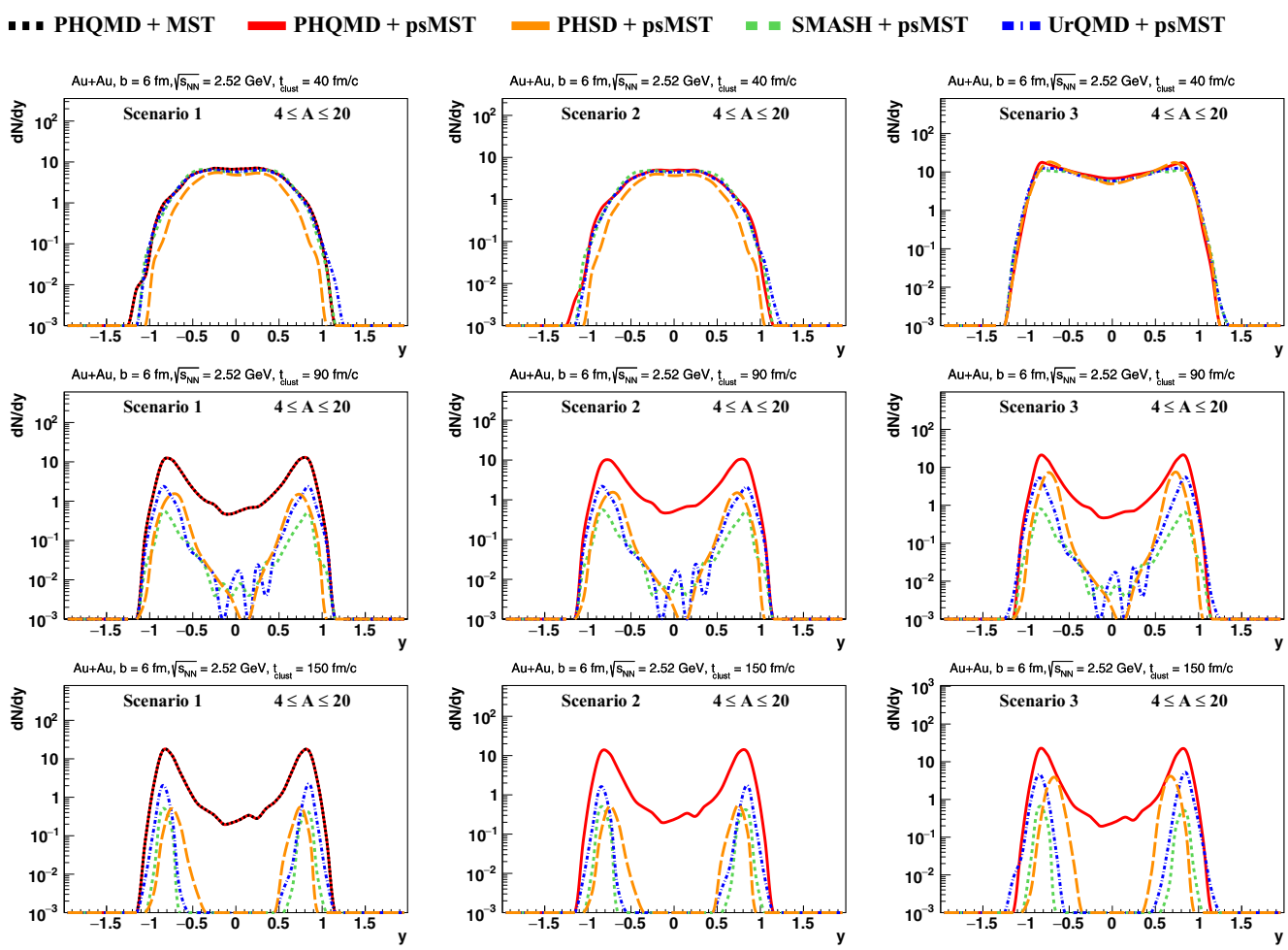

FIG. 7. The rapidity distributions of clusters with the mass number $4 \leqslant A \leqslant 20$ at $t_{\rm clust} = 40, 90, 150$ fm/c in semiperipheral ($b = 6$ fm) Au + Au collisions at $\sqrt{s} = 2.52$ GeV. The left column shows scenario 1, the center column shows scenario 2, the right column shows scenario 3. The color coding is the same as in Fig. 3.

UrQMD, used in this study, contains also particles under formation time and those are also included in the cluster-finding procedure. The PHSD and PHQMD provide a separate output for the formed baryons only, used for the clusters recognition algorithm. A study with PHQMD shows that including unformed nucleons in the MST, additionally to the formed nucleons, gives only small differences at early time steps.

IV. RESULTS FOR THE CLUSTER FORMATION

Figure 1 presents the results of calculations for the rapidity spectra of $A = 1$ baryons (p, n, Λ, and Σ^0) in semiperipheral ($b = 6$ fm) Au + Au collisions at $\sqrt{s} = 2.52$ GeV (scenario 1). The left plot represents the distributions at 40 fm/c, the central column—at 90 fm/c, the right column—at 150 fm/c.

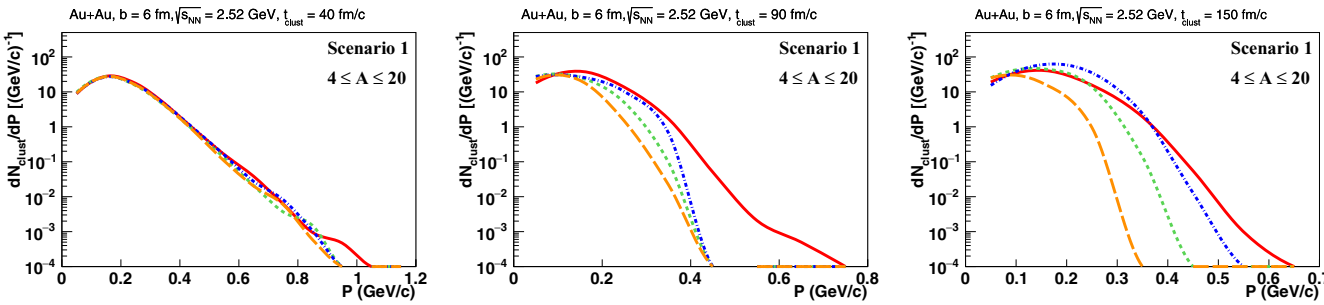

FIG. 8. The momentum spectra of baryons (p, n, Λ, and Σ^0) from $4 \leqslant A \leqslant 20$ clusters in semiperipheral ($b = 6$ fm) Au + Au collisions at $\sqrt{s} = 2.52$ GeV (integrated over all rapidity range). The momentum is calculated in the cluster center-of-mass frame. The left column shows $t_{\rm clust} = 40$ fm/c, the center column shows $t_{\rm clust} = 90$ fm/c, the right column shows $t_{\rm clust} = 150$ fm/c. The color coding is the same as in Fig. 3.

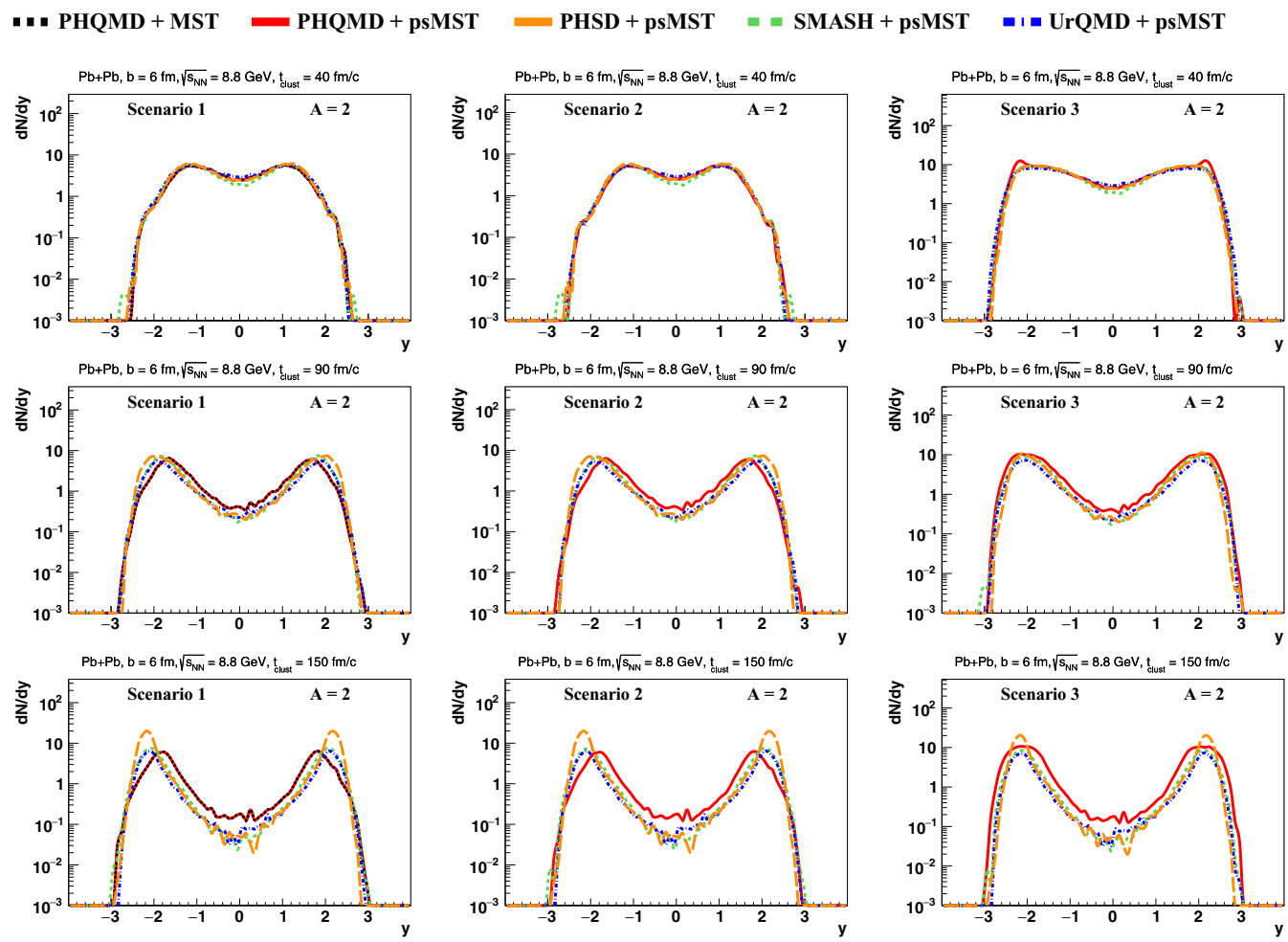

FIG. 9. The rapidity distributions of clusters with the mass number $A = 2$ in semiperipheral ($b = 6$ fm) Pb + Pb collisions at $\sqrt{s} = 8.8$ GeV at $t_{\rm clust} = 40$, 90, 150 fm/c. The left column shows scenario 1, the center column shows scenario 2, the right column shows scenario 3. The color coding is the same as in Fig. 3.

The red solid lines show the PHQMD results, the orange long dashed lines indicate the PHSD results, the green dashed lines correspond to the SMASH results, and the blue dot-dashed lines show the UrQMD predictions.

The rapidity spectra for Pb + Pb collisions at $\sqrt{s} =$ 8.8 GeV are shown in Fig. 2; the colors are the same as in Fig. 1. It is very remarkable that all four transport approaches give a very similar rapidity distribution and hence a very similar stopping despite of the complexity of this process. That is important for our study of clusters since they are more sensitive to the spatial and momentum correlations than single-particle observables.

Next comes the rapidity spectra of clusters with mass number $A = 2$ in semiperipheral ($b = 6$ fm) Au + Au collisions at

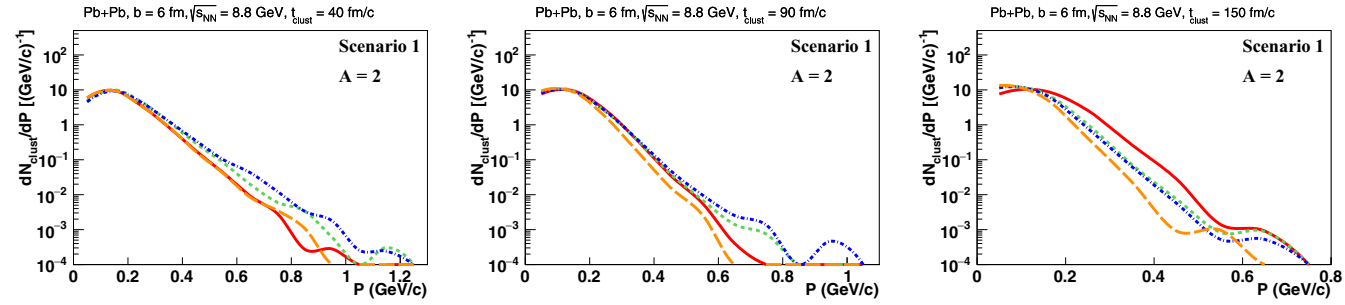

FIG. 10. The momentum spectra of baryons (p, n, Λ, and Σ^0) in $A = 2$ clusters in semiperipheral ($b = 6$ fm) Pb + Pb collisions at $\sqrt{s} = 8.8$ GeV (integrated over all rapidity range). The momentum is calculated in the cluster center-of-mass frame. The left column shows $t_{\rm clust} = 40$ fm/c, the center column shows $t_{\rm clust} = 90$ fm/c, the right column shows $t_{\rm clust} = 150$ fm/c. The color coding is the same as in Fig. 3.

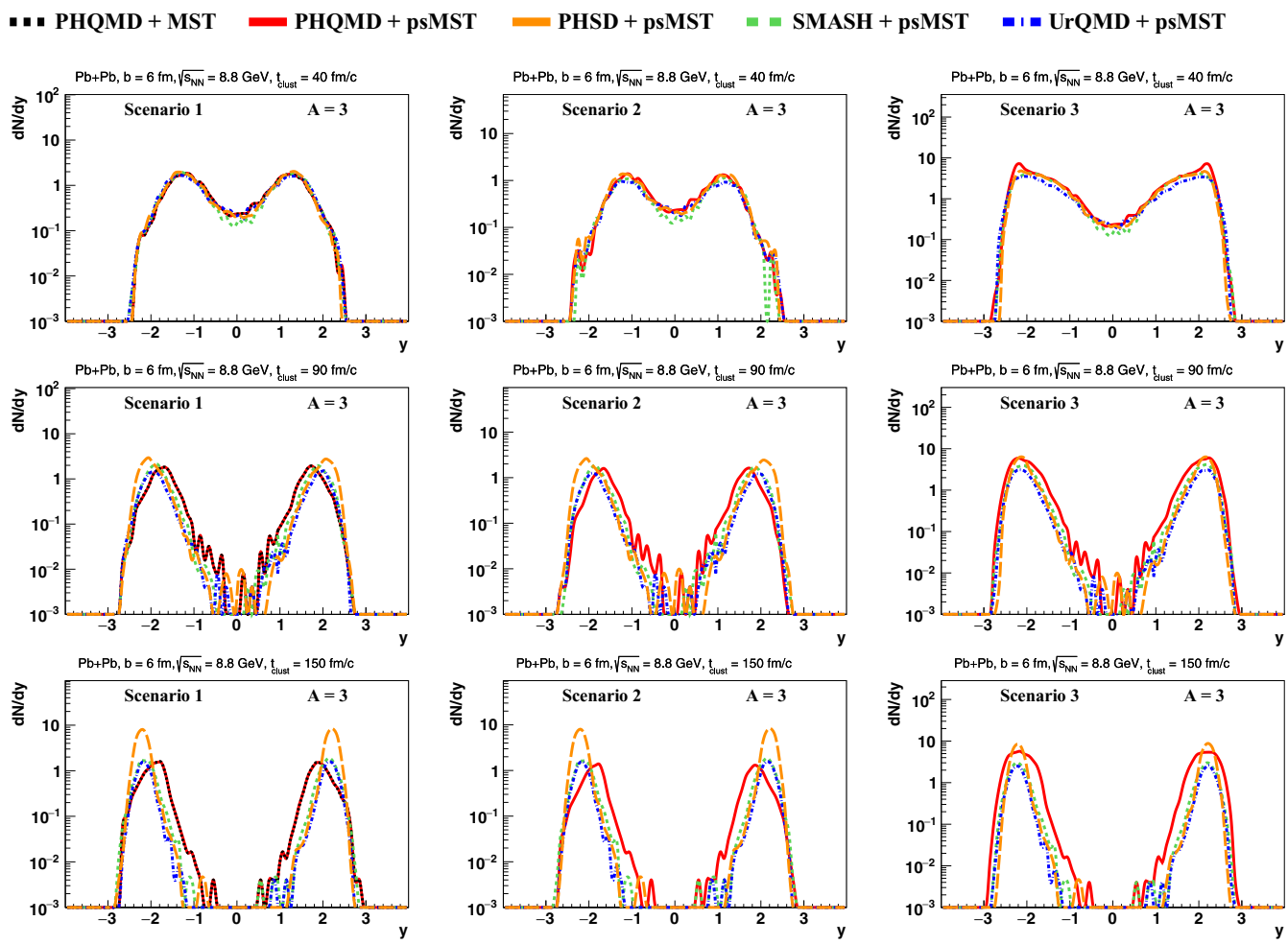

FIG. 11. Rapidity distributions of clusters with the mass number $A = 3$ at $t_{\rm clust} = 40$, 90, 150 fm/c in semiperipheral ($b = 6$ fm) Pb + Pb collisions at $\sqrt{s} = 8.8$ GeV. The left column shows scenario 1, the center column shows scenario 2, the right column shows scenario 3. The color coding is the same as in Fig. 3.

$\sqrt{s} = 2.52$ GeV, which are shown in Fig. 3 for different scenarios for the cluster recognition: the left column corresponds to scenario 1 (see Sec. II), the central column to scenario 2, and the right column to scenario 3. In the upper row the cluster analysis is applied at $t_{\rm clust} = 40$ fm/c, in the middle row at $t_{\rm clust} = 90$ fm/c, and in the lower row at $t_{\rm clust} = 150$ fm/c. The red solid lines show PHQMD results with psMST, the orange long dashed lines indicate results of PHSD with psMST, the green dashed lines correspond to SMASH results with psMST, and the blue dot-dashed lines show results of UrQMD with psMST. Additionally, the PHQMD results with its internal MST cluster recognition algorithm as described in Ref. [26] are presented—cf. the back short dashed lines (PHQMD + MST) in the left column of scenario 1. For scenario 1, the

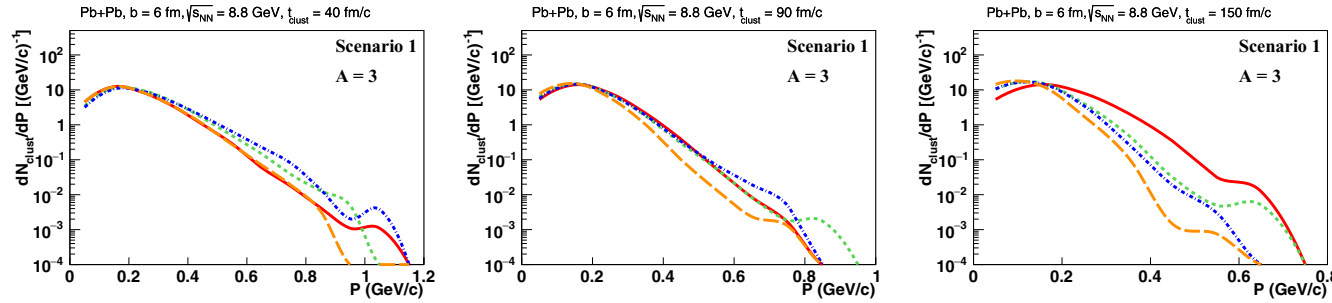

FIG. 12. Momentum spectra of baryons (p, n, Λ, and Σ^0) in $A = 3$ clusters in semiperipheral ($b = 6$ fm) Pb + Pb collisions at $\sqrt{s} = 8.8$ GeV (integrated over all rapidity range). Momentum is calculated in the cluster center-of-mass frame. The left column shows $t_{\rm clust} = 40$ fm/c, the center column shows $t_{\rm clust} = 90$ fm/c, the right column shows $t_{\rm clust} = 150$ fm/c. The color coding is the same as in Fig. 3.

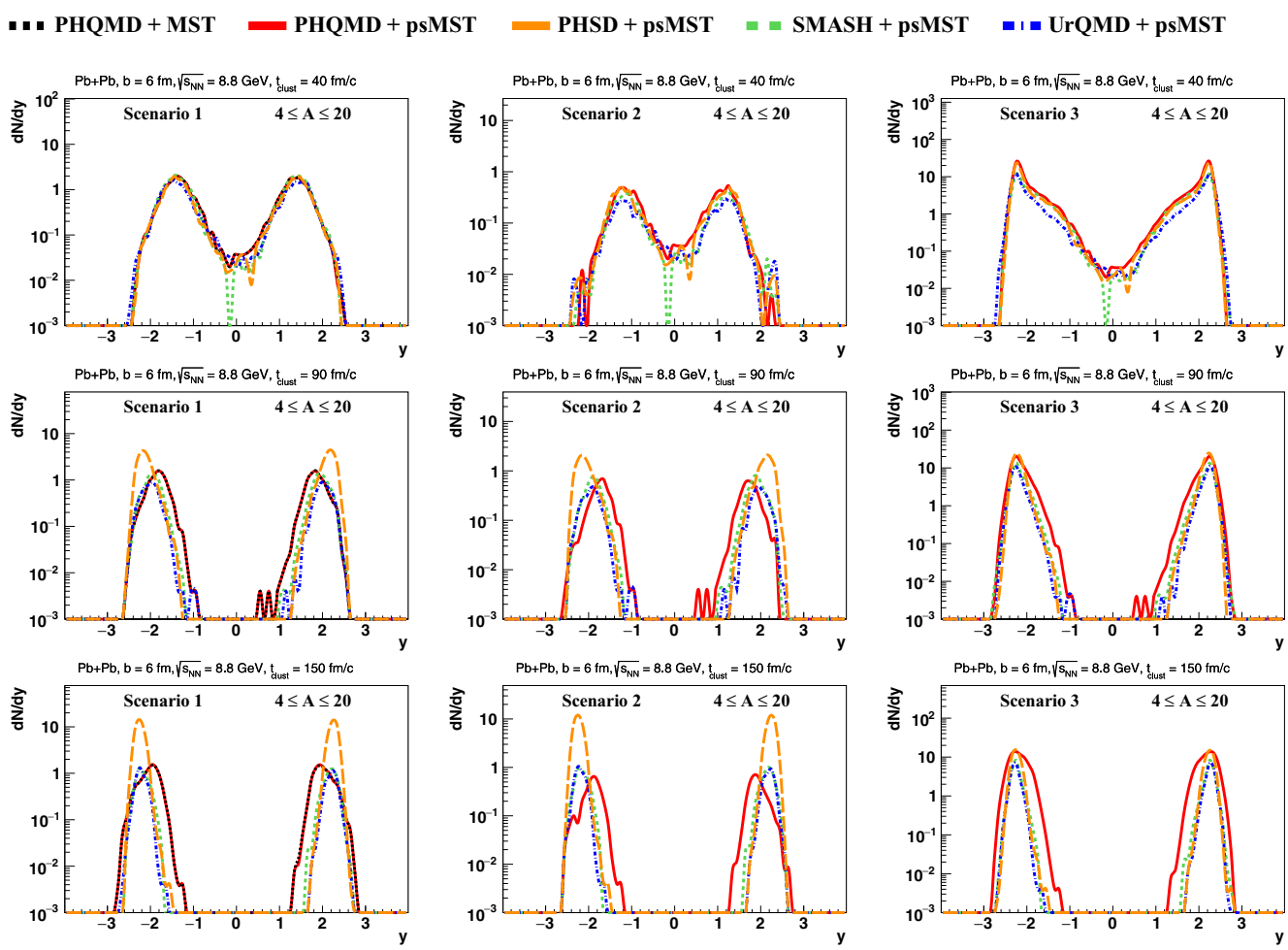

FIG. 13. The rapidity distributions of clusters with the mass number $4 \leqslant A \leqslant 20$ at $t_{\rm clust} = 40$, 90, 150 fm/c in semiperipheral ($b = 6$ fm) Pb + Pb collisions at $\sqrt{s} = 8.8$ GeV. The left column shows scenario 1, the center column shows scenario 2, the right column shows scenario 3. The color coding is the same as in Fig. 3.

results for PHQMD with psMST and that obtained by applying the internal MST algorithm are identical, as expected.

At an early time, $t_{\rm clust} = 40$ fm/c, all models show a similar rapidity distributions, at the later times $t_{\rm clust} = 90,\ 150$ fm/c the PHQMD predicts more clusters in the midrapidity region than the MF-based PHSD approach (with potential) or the cascade approaches, SMASH and UrQMD (without potential). This shows the importance of the n-body dynamics (realized by two-body potential interactions between the baryons in PHQMD) for the cluster formation.

The momentum spectra of baryons in $A = 2$ clusters (integrated over all rapidities) found by psMST within scenario

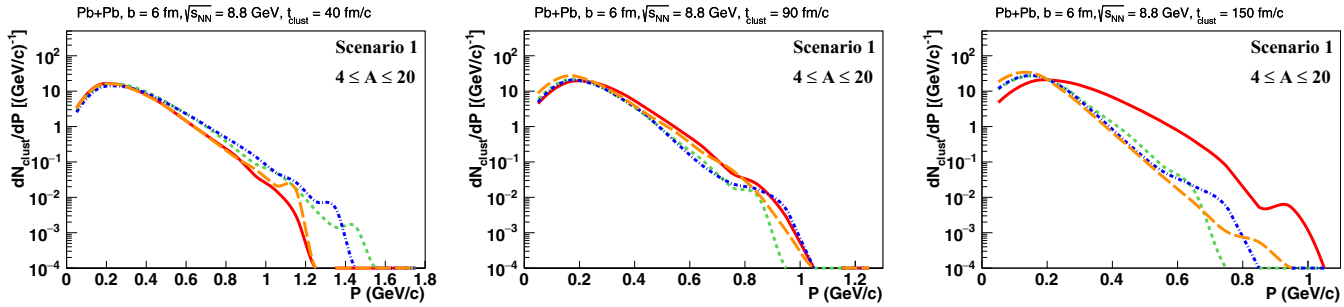

FIG. 14. Momentum spectra of baryons (p, n, Λ, and Σ^0) in $4 \leqslant A \leqslant 20$ clusters in semiperipheral ($b = 6$ fm) Pb + Pb collisions at $\sqrt{s} = 8.8$ GeV (integrated over all rapidity range). Momentum is calculated in the cluster center-of-mass frame. The left column shows $t_{\rm clust} = 40$ fm/c, the center column shows $t_{\rm clust} = 90$ fm/c, the right column shows $t_{\rm clust} = 150$ fm/c. The color coding is the same as in Fig. 3.

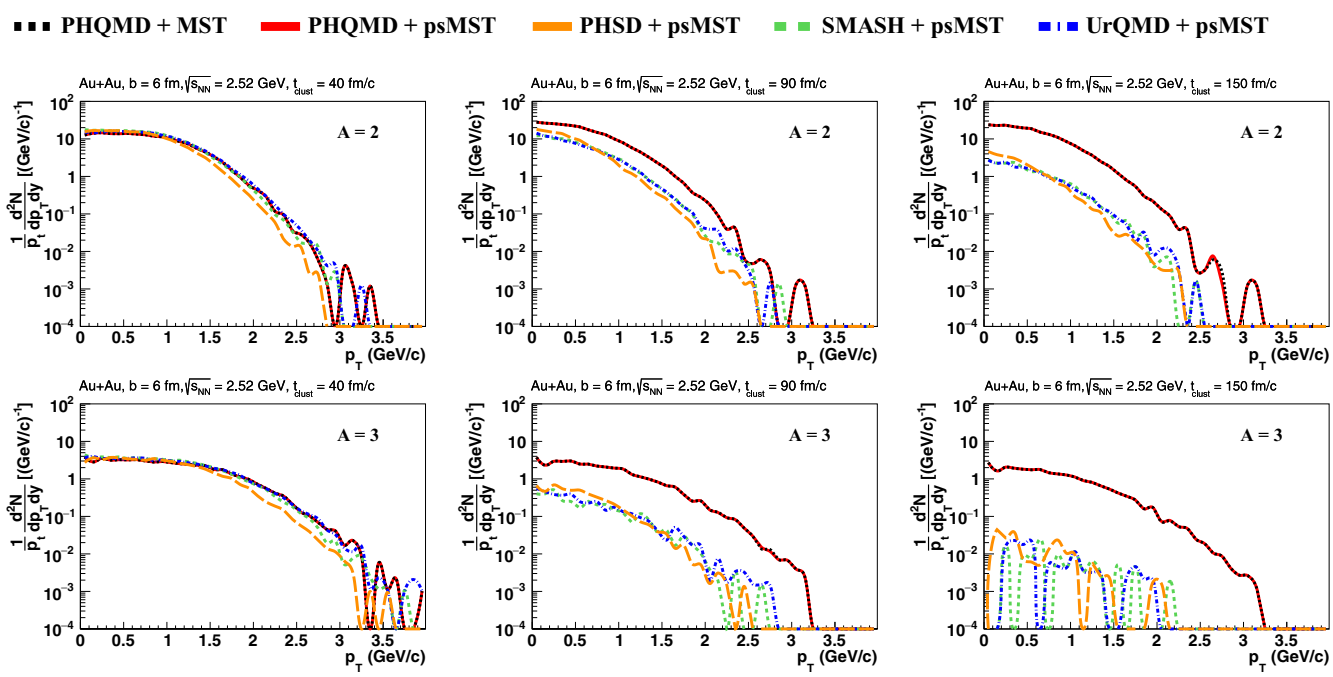

FIG. 15. The transverse momentum spectra of clusters with the mass number $A = 2$ (top row) and $A = 3$ (bottom row) at midrapidity $|y| < 0.5$ in semiperipheral ($b = 6$ fm) Au + Au collisions at $\sqrt{s_{NN}} = 2.52$ GeV. The left column shows $t_{\rm clust} = 40$ fm/c, the middle column shows $t_{\rm clust} = 90$ fm/c, the right column shows $t_{\rm clust} = 150$ fm/c. The color coding is the same as in Fig. 3.

1 in semiperipheral ($b = 6$ fm) Au + Au collisions at $\sqrt{s} = 2.52$ GeV are shown in Fig. 4. Recall that, in this scenario, only coordinate-space information is used to determine the cluster size and that the nucleon momenta are calculated in the cluster center-of-mass frame.

Similar to the rapidity distributions, the momentum distributions at the early time $t_{\rm clust} = 40$ fm/c are very close to each other; however, different dynamics of hadrons leads to a spreading of momentum distributions at later times. Figure 4 also gives an indication of the fraction of clusters which can be discarded by the momentum condition of scenarios 2 and 3.

A similar trend is found for clusters with the mass number $A = 3$, shown in Figs. 5 and 6, and for the intermediate-mass clusters with $4 \leqslant A \leqslant 20$, presented in Figs. 7 and 8: at the lower energy ($\sqrt{s_{NN}} = 2.52$ GeV), PHQMD predicts several orders of magnitude more clusters at midrapidity than the other models of this study. This shows the importance of spatial-momentum correlations which are kept in the QMD dynamics, in contradiction with the MF dynamics where the forces between test particles are reduced by Num, the number of test particles per physical particle.

The picture becomes different at the higher energy: there PHQMD, SMASH, and UrQMD show qualitatively similar results for the rapidity and momentum distributions in semiperipheral ($b = 6$ fm) Pb + Pb collisions at $\sqrt{s_{NN}} = 8.8$ GeV which are presented on Figs. 9–14 for three scenarios. Here the large difference in cluster production between the PHQMD and the other models at midrapidity becomes

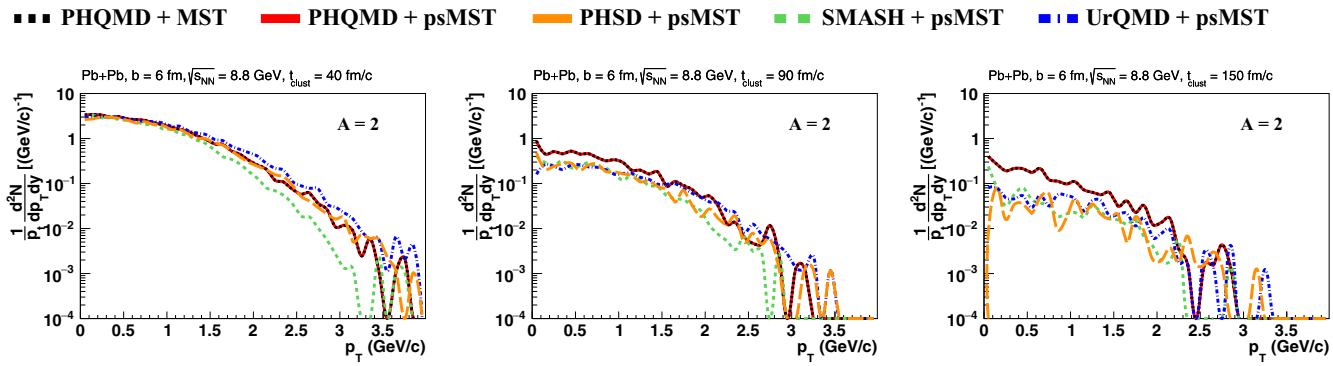

FIG. 16. The transverse momentum spectra of clusters with the mass number $A = 2$ at midrapidity $|y| < 0.5$ in semiperipheral ($b = 6$ fm) Pb + Pb collisions at $\sqrt{s_{NN}} = 8.8$ GeV. The left column shows $t_{\rm clust} = 40$ fm/c, the middle column shows $t_{\rm clust} = 90$ fm/c, the right column shows $t_{\rm clust} = 150$ fm/c. The color coding is the same as in Fig. 3.

much less visible compared with the results for $\sqrt{s_{NN}} = 2.52$ GeV. That can be attributed to the fact that the dynamics at high energy is dominated by collisions rather than by potential interactions. Moreover, the QGP formation is included in the PHSD and the PHQMD explicitly, while the SMASH and the UrQMD are hadronic cascades only.

Finally, the transverse momentum p_T spectra for clusters with the mass number $A = 2$ (top row) and $A = 3$ (bottom row) are presented in Figs. 15 and 16 for $\sqrt{s_{NN}} = 2.52$ GeV and $\sqrt{s_{NN}} = 8.8$ GeV, respectively, at $t_{\rm clust} = 40$ fm/c (left column), $t_{\rm clust} = 90$ fm/c (central column), and $t_{\rm clust} = 150$ fm/c (right column). The transverse momentum spectra are calculated at midrapidity ($|y| < 0.5$). The large splitting of the results for the p_T spectra at later times is attributed to the differences in the rapidity distribution between the PHQMD and other models at low energies, which are large at midrapidity. It should be mentioned that the slopes of the p_T spectra from different models are in a good agreement. Unfortunately, $A = 3$ spectra were affected by insufficient statistics, especially at the higher energy, $\sqrt{s_{NN}} = 8.8$ GeV.

V. CONCLUSIONS

In this study, the results on cluster dynamics within the novel model-independent cluster recognition library for the clusters finding the phase-space minimum spanning tree (psMST) have been presented. The psMST is a tool which can be applied to different transport approaches: the input for psMST are the baryon coordinates and their four-momenta at a selected time. The psMST is based on the MST method for the cluster recognition by correlations in the coordinate space; however, it is extended for the possible inclusion of the momentum-space information, which allows us to study the momentum correlations of baryons in the clusters as well as to modify the criteria for the cluster recognition.

The psMST algorithm has been applied to QMD-based (PHQMD) and mean-field-based (PHSD) transport approaches as well as to two cascade models, SMASH and UrQMD, which are used here without potentials. PHSD incorporated the mean-field potential for baryons and the PHQMD follows the n-body quantum molecular dynamics based on density-dependent two-body interactions.

One finds that the rapidity and momentum distributions of baryons (p, n, Λ, and Σ^0) at early times are very similar within all four models. At later times the rapidity distributions of clusters with $A = 2, 3, [4–20]$ are rather different at low energies. The PHQMD with psMST predicts more clusters in the midrapidity region than the other models. This can be explained by the fact that the n-body quantum molecular dynamics allows us to keep the potential-induced spatial correlations of baryons, contrary to the mean-field dynamics of the PHSD and the cascade versions of SMASH and UrQMD. This observation shows the sensitivity of the clusters production at low energies to the realization of the potential interactions. This sensitivity is much more pronounced for the clusters than for the single-particle observables. At higher energies all models gives qualitatively similar results since the dynamics there is driven mainly by collisions and multiparticle productions rather then by potential interactions.

Note that the psMST library is an open-source tool [27], which can be used in a stand-alone mode or can be integrated into experimental software frameworks. Being applied to different transport models, the psMST might be useful for simulations of the cluster production for experimental studies of detector performances, etc., which are of particular importance for the future experiments of NICA and FAIR.

ACKNOWLEDGMENTS

I would like to acknowledge the theoretical support and discussions with Joerg Aichelin and Elena Bratkovskaya. I would also like to thank Hannah Elfner (Petersen) and Marcus Bleicher for comments and remarks on SMASH and UrQMD models. Also I acknowledge the discussions with Gabriele Coci, Susanne Glaessel, Vadim Kolesnikov, and Vadim Voronyuk. This work was supported by the Russian Science Foundation, Grant No. 19-42-04101 and by the RFBR according to the research Project No. 18-02-40086. Furthermore, I acknowledge support by the Deutsche Forschungsgemeinschaft (DFG, German Research Foundation), Grant No. BR 4000/7-1; by the Helmholtz Research Academy Hesse for FAIR (HFHF), and by Strong-2020, financed by the European community. The author thanks the Giersch Science Center of the J.W. Goethe University for its hospitality.

[1] V. D. Kekelidze, R. Lednicky, V. A. Matveev, I. N. Meshkov, A. S. Sorin, and G. V. Trubnikov, Three stages of the NICA accelerator complex, Eur. Phys. J. A **52**, 211 (2016).

[2] A. Schüttauf *et al.*, Universality of spectator fragmentation at relativistic bombarding energies, Nucl. Phys. A **607**, 457 (1996).

[3] C. Sfienti *et al.* (ALADiN2000 Collaboration), Gross properties and isotopic phenomena in spectator fragmentation, Nucl. Phys. A **787**, 627 (2007).

[4] R. Nebauer *et al.* (INDRA Collaboration), Multifragmentation in Xe(50 AMeV) + Sn: Confrontation of theory and data, Nucl. Phys. A **658**, 67 (1999).

[5] W. Reisdorf *et al.* (FOPI Collaboration), Systematics of central heavy ion collisions in the 1*A* GeV regime, Nucl. Phys. A **848**, 366 (2010).

[6] C. Rappold *et al.*, Hypernuclear production cross section in the reaction of ^{6}Li + ^{12}C at 2*A* GeV, Phys. Lett. B **747**, 129 (2015).

[7] T. Anticic *et al.* (NA49 Collaboration), Production of deuterium, tritium, and ^{3}He in central Pb + Pb collisions at 20*A*, 30*A*, 40*A*, 80*A*, and 158*A* GeV at the CERN Super Proton Synchrotron, Phys. Rev. C **94**, 044906 (2016).

[8] B. I. Abelev *et al.* (STAR Collaboration), Observation of an antimatter hypernucleus, Science **328**, 58 (2010).

[9] H. Agakishiev *et al.* (STAR Collaboration), Observation of the antimatter helium-4 nucleus, Nature (London) **473**, 353 (2011); **475**, 412 (2011).

[10] J. Adam *et al.* (ALICE Collaboration), ${}^{3}_{\Lambda}\mathrm{H}$ and ${}^{3}_{\Lambda}\overline{\mathrm{H}}$ production in Pb-Pb collisions at $\sqrt{s_{\mathrm{NN}}} = 2.76$ TeV, Phys. Lett. B **754**, 360 (2016).

[11] J. Adam *et al.* (ALICE Collaboration), Production of light nuclei and anti-nuclei in pp and Pb-Pb collisions at energies available at the CERN Large Hadron Collider, Phys. Rev. C **93**, 024917 (2016).

[12] S. Acharya *et al.* (ALICE Collaboration), Production of ${}^{4}\mathrm{He}$ and ${}^{4}\overline{\mathrm{He}}$ in Pb-Pb collisions at $\sqrt{s_{\mathrm{NN}}} = 2.76$ TeV at the LHC, Nucl. Phys. A **971**, 1 (2018).

[13] A. S. Botvina, K. K. Gudima, J. Steinheimer, M. Bleicher, and I. N. Mishustin, Production of spectator hypermatter in relativistic heavy-ion collisions, Phys. Rev. C **84**, 064904 (2011).

[14] A. S. Botvina, K. K. Gudima, J. Steinheimer, M. Bleicher, and J. Pochodzalla, Formation of hypernuclei in heavy-ion collisions around the threshold energies, Phys. Rev. C **95**, 014902 (2017).

[15] H. H. Gutbrod, A. Sandoval, P. J. Johansen, A. M. Poskanzer, J. Gosset, W. G. Meyer, G. D. Westfall, and R. Stock, Final State Interactions in the Production of Hydrogen and Helium Isotopes by Relativistic Heavy Ions on Uranium, Phys. Rev. Lett. **37**, 667 (1976).

[16] J. Gosset, H. H. Gutbrod, W. G. Meyer, A. M. Poskanzer, A. Sandoval, R. Stock, and G. D. Westfall, Central collisions of relativistic heavy ions, Phys. Rev. C **16**, 629 (1977).

[17] M. C. Lemaire, S. Nagamiya, S. Schnetzer, H. Steiner, and I. Tanihata, Composite particle emission in high-energy heavy ion collisions, Phys. Lett. B **85**, 38 (1979).

[18] H. Sato and K. Yazaki, On the coalescence model for high-energy nuclear reactions, Phys. Lett. B **98**, 153 (1981).

[19] V. Gaebel, M. Bonne, T. Reichert, A. Burnic, P. Hillmann, and M. Bleicher, Understanding the energy dependence of B_2 in heavy ion collisions: Interplay of volume and space-momentum correlations, Eur. Phys. J. A **57**, 55 (2021).

[20] S. Sombun, K. Tomuang, A. Limphirat, P. Hillmann, C. Herold, J. Steinheimer, Y. Yan, and M. Bleicher, Deuteron production from phase-space coalescence in the UrQMD approach, Phys. Rev. C **99**, 014901 (2019).

[21] J. Aichelin, "Quantum" molecular dynamics—A dynamical microscopic n-body approach to investigate fragment formation and the nuclear equation of state in heavy ion collisions, Phys. Rep. **202**, 233 (1991).

[22] R. K. Puri, C. Hartnack, and J. Aichelin, Early fragment formation in heavy ion collisions, Phys. Rev. C **54**, R28(R) (1996).

[23] R. K. Puri and J. Aichelin, Simulated annealing clusterization algorithm for studying the multifragmentation, J. Comput. Phys. **162**, 245 (2000).

[24] C. Dorso and J. Randrup, Early recognition of clusters in molecular dynamics, Phys. Lett. B **301**, 328 (1993).

[25] A. Le Fèvre, J. Aichelin, C. Hartnack, and Y. Leifels, FRIGA: A new approach to identify isotopes and hypernuclei in n-body transport models, Phys. Rev. C **100**, 034904 (2019).

[26] J. Aichelin, E. Bratkovskaya, A. Le Fèvre, V. Kireyeu, V. Kolesnikov, Y. Leifels, V. Voronyuk, and G. Coci, Parton-hadron-quantum-molecular dynamics: A novel microscopic n-body transport approach for heavy-ion collisions, dynamical cluster formation, and hypernuclei production, Phys. Rev. C **101**, 044905 (2020).

[27] https://gitlab.com/vkireyeu/psmst

[28] W. Cassing and E. L. Bratkovskaya, Parton transport and hadronization from the dynamical quasiparticle point of view, Phys. Rev. C **78**, 034919 (2008).

[29] W. Cassing and E. L. Bratkovskaya, Parton-hadron-string dynamics: An off-shell transport approach for relativistic energies, Nucl. Phys. A **831**, 215 (2009).

[30] W. Cassing, Dynamical quasiparticles properties and effective interactions in the sQGP, Nucl. Phys. A **795**, 70 (2007).

[31] W. Cassing, QCD thermodynamics and confinement from a dynamical quasiparticle point of view, Nucl. Phys. A **791**, 365 (2007).

[32] J. Weil *et al.*, Particle production and equilibrium properties within a new hadron transport approach for heavy-ion collisions, Phys. Rev. C **94**, 054905 (2016).

[33] D. Oliinychenko, V. Steinberg, J. Weil, J. Staudenmaier, M. Kretz, A. Schäfer, H. E. (Petersen), S. Ryu, J. Rothermel, J. Mohs, F. Li, A. Sorensen, D. Mitrovic, L. Pang, J. Hammelmann, A. Goldschmidt, M. Mayer, O. Garcia-Montero, N. Kübler, and Nikita, smash-transport/smash: Smash-2.0 (2020), https://zenodo.org/record/4336358/export/hx.

[34] S. A. Bass *et al.*, Microscopic models for ultrarelativistic heavy ion collisions, Prog. Part. Nucl. Phys. **41**, 255 (1998).

[35] M. Bleicher *et al.*, Relativistic hadron hadron collisions in the ultrarelativistic quantum molecular dynamics model, J. Phys. G **25**, 1859 (1999).